Astron. Astrophys. 229, 362–377 (1990)

ASTRONOMY AND ASTROPHYSICS

Small-scale structures in the H I distribution of M 33

E.R. Deul and R.H. den Hartog

Sterrewacht Leiden, Postbox 9503, NL-2300 RA Leiden, The Netherlands

Received September 1, 1988; accepted January 12, 1989

Abstract. Recent high-resolution H I observations of M 33 reveal a large number of regions that are devoid of emission. We interpret these regions as holes formed by interstellar winds; a catalogue containing 148 of these H I holes has been compiled. Their diameters range from the survey resolution limit (>40 pc) to 1 kpc. The swept-up mass, estimated from surrounding H I densities, ranges from 10^3 $M_\odot$ to 10^7 $M_\odot$. Energies needed to excavate such holes are between 10^{49} to 10^{54} erg. Indicative ages, based on derived expansion velocities and diameters, show a cutoff near $7\,10^6$ yr. Three statistical analysis techniques are applied to determine positional correlation of the H I holes with H II regions, OB associations, and supernova remnants. These techniques use correlation distances, percolation, and overlap parameters to establish correlation. Small ($D<200$ pc) H I holes correlate well with OB associations and to a lesser extent with H II regions. The giant H II regions NGC 604, NGC 595, and IC 133 coincide with small, high-contrast H I holes of similar morphology. The large ($D>500$ pc) holes show an anti-correlation, in the sense that the H II regions and OB associations lie on the hole edges. These holes are generally interarm cavities. If smaller holes are supernova induced, the implied supernova rate of 3 per 1000 years is within the errors of determinations by Tammann and Berkhuijsen. Alternatively, if the deficiency of H I line emission is due to a conversion of atomic to molecular hydrogen, ^{12}CO emission should be observable assuming the galactic conversion factor between integrated CO brightnesses and molecular hydrogen column density. In four holes, CO emission was searched for, but not found. This is either due to a smaller ($<0.3\times$ the galactic) CO-to-H_2 conversion factor, or due to a molecular cloud mass smaller than that expected from the atomic hydrogen densities around the hole. The surface filling factor of all holes, multiplied by 2 to account for non-detected holes, is $<40\%$, which is small compared to the value given by McKee and Ostriker.

Key words: galaxies: general – galaxies: structure of – interstellar medium: bubbles – interstellar medium: general – radio lines: 21-cm

1. Introduction

Neutral atomic hydrogen observations of M 33, described by Deul and van der Hulst (1986), reveal a multitude of fine-scale structures. The filamentary nature of the H I distribution shows great similarity to that of our own Galaxy. Inspection of the neutral atomic hydrogen distribution in M 33 on a television image display reveals the wealth of detail and complexity of this distribution. To infrared astronomers, these structures would resemble an ensemble of cirrus features. At many places the filaments seem to form loops or holes. Therefore, an alternative view would simplify the H I distribution to a homogeneous layer containing a large number of holes. The M 33 H I holes are comparable to the (super) giant H I shells in the Galaxy (Heiles, 1979; 1984) and the LMC (Meaburn, 1980) and are very similar to the H I holes in M 31 (Brinks and Bajaja, 1986). In most cases we do not resolve the shell structure itself, so that we prefer the terminology: holes.

The observations suggest that the H I shells/holes are characteristic of the late type spiral galaxies in the Local Group. They may exist in all late type spirals (e.g. M 101, Viallefond et al., 1981). There are two competing types of theories to explain the origin of holes and shells in the interstellar medium. The first type relies on wind pressure to excavate cavities; the energy source could be stellar mass loss (Castor et al., 1975; Weaver et al., 1977), supernova explosions (Chevalier, 1977) or both (Bruhweiler et al., 1980; Tomisaka et al., 1981; McCray and Kafatos, 1987). This type also includes the H I holes of a few hundred pc in diameter that may be the result of normal H II region evolution (Tenorio-Tagle et al., 1982; Tenorio-Tagle, 1984). Existing H I shells may expand to become supershells by the radiation pressure of field stars (Elmegreen and Chiang, 1982). In fact these theories describe an evolutionary track for H I shells, from 20 pc diameters to >1 kpc sizes. The second type involves collisions between high-velocity clouds and a galactic disk to create structures reminiscent of shells in the quiescent H I layer (Tenorio-Tagle, 1981).

Alternatively, holes may be places where atomic hydrogen gas has been converted into molecular form, causing the absence of neutral atomic hydrogen emission. We will consider this possibility in Sect. 3.3.

In the Milky Way the unfavorable position of the observer causes considerable line-of-sight blending problems. The high inclination of M 31 together with the distribution of the H I emission in a narrow ring structure also makes studies of the H I shell/hole phenomenon improper. M 33, however, is better suited to investigate the H I hole phenomenon. The resolution limit of our H I observations (40 pc) allows investigation of the hydrogen morphology on scales comparable to the sizes of H II regions and OB associations. In particular the large H II regions should be observable as small H I holes.

We have compiled a catalogue of H I holes in M 33, determined the characteristics of the H I holes ensemble, and correlated the observed holes with other objects known to influence

Send offprint requests to: E.R. Deul

the physical properties of the surrounding interstellar medium. Details of identification and classification and the general characteristics of the H I hole distribution are presented in Sect. 2. We describe the various correlations in Sect. 3. Section 4 discusses the implications of the correlations found.

2. The H I hole catalogue

In this section we first describe the H I hole catalogue and parameters that can be derived from examination of the individual channel maps of the M 33 H I survey. Next we discuss the influence of the selection criteria on the derivation of the catalogue in detail. Physically meaningful cross correlations between the observed and derived parameters are presented in Sect. 2.2.

2.1. The catalogue

Ideally, one would like to have an automatic routine for the detection and classification of H I holes in order to avoid any subjective influence in their recognition. Hu (1981) was able to create a special purpose filter for the H I observations of our own Galaxy. This particular scheme, that detects the edge structures of H I shells, cannot be applied to the M 33 H I survey, because our large beam (40 pc, FWHM) does not resolve shell edges from background emission. To minimize subjective factors such as prejudice and human-eye pattern recognition, which are inherent to visual inspection, we adopt here the selection criteria, definition, description, and classification of H I holes by Brinks and Bajaja (1986). This has the advantage that it allows direct comparison between M 31 and M 33 results. The criteria are: (i) A H I hole must persist over at least three consecutive channel maps. This criterion should eliminate noise on the scale of the beam. Holes appearing in only two channels are rejected because neighboring channels are not independent as a result of the Hanning taper used. (ii) The position of a H I hole should not change among channel maps. Kinematical effects and noise structures may cause such changes. (iii) The contrast of the hole with its surroundings must be good. Stated in this way, this criterion is subjective, but we use it as a first order selection requirement that will later be quantified by examining the intensities between the hole center and its surroundings. (iv) The hole shape must be clearly defined and adequately described by an ellipse. This criterion necessarily limits the expected shape of the objects we try to find. Use of these criteria thus emphasizes detection confidence at the expense of completeness.

We searched the individual channel maps (see Deul and van der Hulst, 1986) for holes by visual inspection. The noise in the maps is independent of position so that the search for holes is uniform throughout the map area with respect to the noise level.

Both authors independently compiled lists of candidate objects. To minimize systematic effects, we searched the individual channel maps going from negative to positive velocities, as well as in the reversed order. Each hole candidate was given a quality rating, Q, depending on the number of criteria met. For the candidate objects we estimated central positions, angular sizes, eccentricity, position angle of the major axis, and the velocity at which the hole shows maximum contrast. Most of these parameters were derived using a special purpose computer routine allowing interactive interfacing between the image display and the user. Candidate lists were compared and combined to create the final list of H I holes. Comparing the candidate list, we found the quality rating to be dependent on personal bias. For a candidate object to be part of the final list it must appear in both candidate lists with the following requirements: between the two lists the difference in (i) position should be less or equal to two resolution elements, (ii) velocity of maximum contrast should be less than two channels, (iii) quality rating should be less than two, and (iv) angular size should be less than 10%.

We identify three types of holes. Type 1 can be seen as an intensity minimum over the full velocity range in position-velocity maps, i.e. a gap in the continuous distribution. Type 2 is seen in the position-velocity maps as a shift in velocity of the H I intensities. Type 3 appears as a valley in the position-velocity maps, splitting the H I velocity structure into two components. Figures 1a, b, and c shows these definitions schematically. To record the completeness of a hole in the channel map of maximum contrast in terms of its circumference, we also obtained the class code C for each hole; "c" for complete and "p" for partial.

To obtain physically meaningful parameters from the observed characteristics, we derive the following values for each hole. (i) The distance with respect to the Galaxy center, together with the position angle defined from the equatorial north pole in the anti-clockwise direction. (ii) The values for the major and

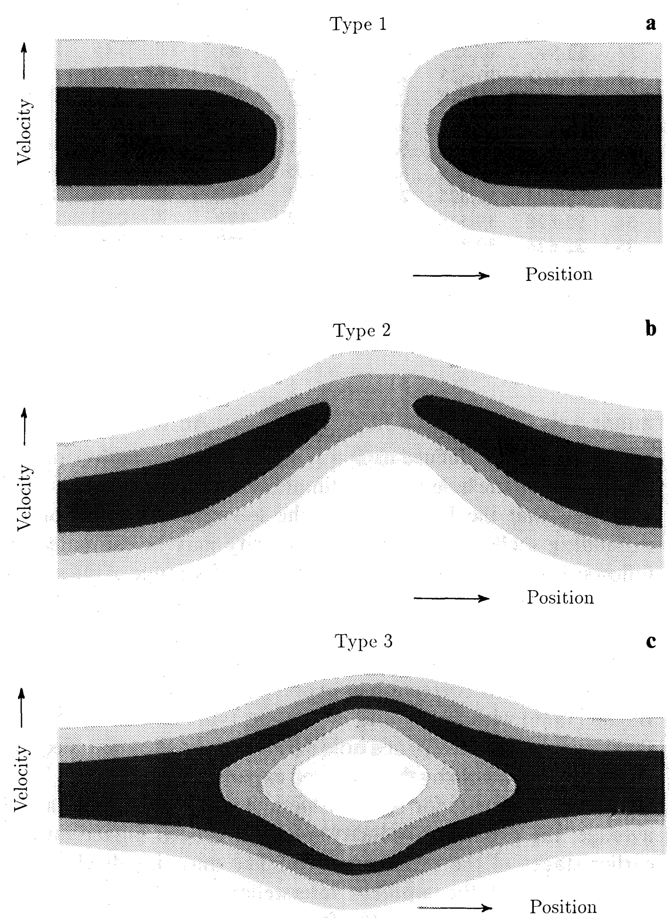

Fig. 1a–c. Schematic diagram of Type difinitions. **a** Type 1 hole showing a gap in the position-velocity map over the entire velocity range. **b** Type 2 hole seen as a shift in velocity in the position-velocity map. The shift may occur both in positive as well as in negative direction. **c** Type 3 holes appear as a local depression in the position-velocity map, splitting the H I velocity structure into two components

Table 1. Properties of the H I holes in the catalogue

no.	$\alpha_{(1950)}$ deg	$\delta_{(1950)}$ deg	R kpc	Θ deg	V_{cen} km s^{-1}	DV km s^{-1}	Cont.	T	Q	C	Minor pc	Major pc	Diam pc	ϵ	p.a. deg	Age 10^6 yr	n_{HI} at cm^{-3}	Mass 10^4 $M_\odot$	Energy 10^{50} ergs
1	22.410	30.183	6.618	37.3	-110	12	0.45	1	2	c	290	400	341	0.689	10	13.9	0.63	32.4	94.2
2	22.448	30.272	5.947	28.6	-130	12	0.41	1	2	c	260	370	310	0.711	7	12.7	1.14	44.1	135.9
3	22.450	30.438	6.617	8.6	-162	22	0.43	2	1	c	90	200	134	0.893	20	3.0	0.44	1.4	8.1
4	22.469	30.205	5.486	39.6	-117	14	0.28	2	2	p	450	720	569	0.781	-13	19.9	0.44	105.9	389.2
5	22.478	30.160	5.406	47.1	-107	9	0.47	3	2	c	210	300	251	0.714	-40	13.7	1.46	29.8	61.8
6	22.481	30.433	5.938	8.8	-170	9	0.30	1	1	p	250	300	274	0.553	-5	14.9	0.32	8.4	14.7
7	22.507	30.430	5.389	8.8	-175	15	0.32	2	1	p	110	180	141	0.792	-10	4.6	0.76	2.7	10.0
8	22.514	30.316	4.703	26.1	-133	8	0.43	3	1	c	70	120	92	0.812	5	5.6	0.44	0.4	0.6
9	22.520	30.359	4.730	19.2	-140	14	0.41	3	2	c	110	160	133	0.726	40	4.6	0.57	1.7	5.5
10	22.530	30.537	5.746	-4.6	-187	13	0.45	1	2	p	830	1650	1170	0.864	-30	44.1	0.51	1052.2	3860.7
11	22.526	30.277	4.404	33.8	-133	-22	0.39	2	2	c	150	250	194	0.800	20	4.3	0.97	9.1	60.9
12	22.535	30.305	4.254	29.4	-137	-26	0.28	2	2	c	220	370	285	0.804	28	5.4	0.44	13.3	107.3
13	22.528	30.327	4.446	25.0	-150	12	0.45	1	1	p	330	850	530	0.922	-62	21.6	0.38	73.2	210.8
14	22.543	30.354	4.223	21.0	-154	12	0.30	2	2	c	100	140	118	0.700	-10	4.8	0.51	1.1	2.7
15	22.545	30.461	4.802	3.7	-179	5	0.31	1	1	c	100	150	122	0.745	-6	12.0	0.44	1.1	0.8
16	22.545	29.939	6.147	85.4	-92	5	0.41	1	1	p	350	580	451	0.797	-10	44.2	0.57	67.6	58.8
17	22.561	30.201	3.901	53.5	-122	22	0.42	2	1	p	300	350	324	0.515	-70	7.2	0.89	39.1	274.6
18	22.561	30.380	3.958	16.8	-162	22	0.31	2	3	c	160	250	200	0.768	-30	4.5	0.76	7.9	51.3
19	22.566	30.567	5.332	-10.4	-191	12	0.45	1	3	c	750	1550	1078	0.875	-30	44.0	0.44	720.0	2301.6
20	22.567	30.271	3.629	39.9	-129	12	0.45	3	2	c	70	100	84	0.714	-10	3.4	0.51	0.4	0.9
21	22.570	30.235	3.640	48.3	-112	-23	0.23	2	2	c	100	180	134	0.831	34	2.9	1.08	3.4	23.2
22	22.577	30.251	3.472	46.1	-113	-17	0.25	2	1	c	50	100	71	0.866	-23	2.0	0.76	0.3	1.4
23	22.582	30.321	3.351	30.6	-137	12	0.41	3	1	c	90	120	104	0.661	0	4.2	0.44	0.6	1.6
24	22.586	30.289	3.248	38.9	-129	20	0.46	1	2	c	500	1050	725	0.879	30	17.8	1.01	499.5	3436.8
25	22.592	30.200	3.443	60.9	-113	-10	0.24	2	2	c	100	180	134	0.831	-20	6.6	0.97	3.1	6.5
26	22.592	30.219	3.352	56.7	-125	12	0.23	2	2	c	70	140	99	0.866	0	4.0	0.76	1.0	2.4
27	22.595	30.522	4.320	-7.9	-195	22	0.45	1	2	c	300	650	442	0.887	-30	9.8	0.66	73.5	517.1
28	22.592	30.423	3.565	8.6	-175	15	0.30	2	1	p	500	650	570	0.639	-5	18.6	0.32	76.0	295.5
29	22.593	30.610	5.270	-17.2	-210	11	0.31	3	1	c	180	380	262	0.881	5	11.7	0.57	13.2	32.5
30	22.608	30.492	3.766	-4.8	-187	7	0.23	1	1	c	150	200	173	0.661	25	12.1	0.63	4.3	5.4
31	22.613	30.635	5.201	-21.7	-220	14	0.29	3	2	p	180	320	240	0.827	-25	8.4	0.63	11.3	39.2
32	22.622	30.642	5.144	-23.5	-208	14	0.41	3	1	p	100	180	134	0.831	25	4.7	0.32	1.0	2.9
33	22.625	30.325	2.513	35.7	-145	8	0.45	1	2	p	320	420	367	0.648	-5	22.5	0.57	36.4	59.7
34	22.626	30.515	3.652	-10.2	-199	7	0.23	1	1	c	70	130	95	0.843	-15	6.7	0.32	0.4	0.4
35	22.626	30.620	4.808	-22.2	-230	20	0.41	2	1	c	70	130	95	0.843	-18	2.3	0.32	0.4	1.7
36	22.636	30.029	4.755	-82.3	-88	-10	0.41	2	1	p	330	450	385	0.680	-10	18.9	0.57	42.3	95.3
37	22.637	30.241	2.593	64.9	-120	10	0.41	3	2	c	90	150	116	0.800	10	5.7	0.25	0.5	0.9

minor axis of the ellipse fit to a hole. (iii) An estimate for the effective diameter defined as $D=\sqrt{\text{major} \times \text{minor}}$ and (iv) for the eccentricity of the hole. (v) An estimate of the expansion velocities; assuming that the H I holes are the low-resolution version of expanding shells, their expansion velocity may be estimated as follows: Type 1 holes by examining the velocity range of the gap in the position-velocity diagram; Type 2, from the velocity offset of the H I profile at the center of the hole; Type 3 half of the separation velocity. (vi) The ambient neutral hydrogen density using a geometric correction as expressed in Eq. (1) of Brinks and Bajaja (1986) with $i=57°$ and $h=100$ pc. (vii) An estimate of the maximum kinematic age of a hole derived by dividing the effective radius, $D/2$, of a hole by the observed expansion velocity DV. This is an upper estimate for the true lifetime of the hole, because on average, the expansion velocity must have been higher during earlier stages of the expansion. (viii) The mass involved in the sweeping up of the ambient interstellar material derived by assuming spherical symmetry for the H I hole. Note that the larger holes ($D>500$ pc) will have considerably less mass than derived here, because for a scale height of 100 pc the ambient density will have dropped to 10% at the higher z heights. This also causes the hole to be shaped like a cylinder rather than a sphere. (ix) Finally an estimate of the energy needed to create a cavity of the observed diameter in the H I distribution. We use Heiles's (1979) Eq. (2) for expanding shells to derive this energy, assuming that the ambient density outside the hole represents the density in the hole region before it was created, and assuming that the observed DV velocities are a good estimate of the expansion velocity of the shell structure. Again, this determination assumes spherical symmetry which we know not to be valid for the larger holes.

The observational and derived parameters for each hole are listed in Table 1. The separate columns record the following information.

Column (1): Number of the hole, according to right ascension of the central position.

Column (2): Center position in right ascension and declination coordinates (epoch 1950). The values are accurate to one picture element (12″).

Column (4): Distance of the H I hole with respect to the M 33 center. We have used the central position from Table 1 of Deul and van der Hulst (1986).

Column (5): Orientation angle of the H I holes in the galaxy with respect to the north equatorial pole, with positive sense in the anti-clockwise direction.

Table 1 (continued)

no.	$\alpha_{(1950)}$ deg	$\delta_{(1950)}$ deg	R kpc	Θ deg	V_{cen} km s^{-1}	DV km s^{-1}	Cont.	T	Q	C	Minor pc	Major pc	Diam pc	ε	p.a. deg	Age 10^6 yr	n_{HI} at cm^{-3}	Mass 10^4 $M_\odot$	Energy 10^{50} ergs
38	22.642	30.052	4.465	-82.9	-92	-16	0.30	2	3	c	90	160	120	0.827	35	3.7	1.39	3.1	13.2
39	22.649	30.718	5.659	-32.2	-232	17	0.39	3	1	p	180	320	240	0.827	0	6.9	0.32	5.7	23.7
40	22.650	30.490	2.929	-9.4	-191	8	0.20	1	2	c	140	250	187	0.828	-15	11.5	0.57	4.8	7.3
41	22.650	30.608	4.260	-24.9	-224	24	0.33	2	3	c	90	140	112	0.766	-15	2.3	0.38	0.7	4.4
42	22.651	30.540	3.437	-17.6	-207	20	0.23	2	2	c	120	200	155	0.800	-35	3.8	0.25	1.2	5.9
43	22.656	30.250	2.304	69.8	-117	25	0.43	2	1	c	120	170	143	0.708	40	2.8	0.70	2.6	19.5
44	22.657	30.650	4.677	-29.4	-228	12	0.36	3	1	c	200	380	276	0.850	-25	11.3	0.51	13.8	37.9
45	22.661	30.590	3.854	-25.3	-224	-14	0.22	2	1	c	100	150	122	0.745	5	4.3	0.32	0.8	2.2
46	22.665	30.611	4.051	-27.8	-210	17	0.41	3	2	c	80	120	98	0.745	-20	2.8	0.32	0.4	1.4
47	22.663	30.326	1.804	45.3	-142	21	0.45	1	2	p	700	1100	877	0.771	90	20.5	0.78	687.6	5027.1
48	22.666	30.625	4.212	-29.2	-228	16	0.33	1	1	c	100	160	126	0.781	-5	3.9	0.13	0.3	1.1
49	22.670	30.640	4.334	-31.1	-232	6	0.15	1	1	c	100	100	100	0.000	0	8.2	0.32	0.4	0.4
50	22.670	30.738	5.617	-36.4	-236	18	0.43	3	3	p	160	250	200	0.768	-30	5.4	0.57	5.9	28.1
51	22.671	30.216	2.476	85.4	-109	-26	0.46	2	1	c	330	980	569	0.942	-5	10.7	0.34	81.5	690.4
52	22.671	30.546	3.167	-22.3	-216	16	0.42	2	2	c	140	240	183	0.812	-20	5.6	0.60	4.8	19.0
53	22.676	30.472	2.234	-10.2	-180	16	0.41	3	1	p	120	180	147	0.745	15	4.5	0.38	1.6	5.8
54	22.681	30.302	1.634	64.2	-135	16	0.39	2	1	c	80	130	102	0.788	0	3.1	0.32	0.4	1.5
55	22.687	30.479	2.112	-14.5	-203	15	0.36	2	2	c	110	200	148	0.835	10	4.8	0.51	2.1	7.5
56	22.690	30.502	2.316	-20.1	-207	-13	0.26	2	1	c	140	220	175	0.771	0	6.6	0.60	4.2	12.4
57	22.691	30.422	1.496	3.3	-191	18	0.30	2	1	p	120	280	183	0.904	-10	5.0	0.32	2.5	11.1
58	22.700	30.583	3.151	-33.5	-236	6	0.33	1	2	c	150	330	222	0.891	-30	18.2	0.54	7.7	7.9
59	22.700	30.367	1.081	38.1	-137	-16	0.30	2	1	c	130	150	140	0.499	20	4.3	0.19	0.7	2.3
60	22.701	30.441	1.444	-6.4	-187	-22	0.30	2	2	c	150	250	194	0.800	-15	4.3	0.32	3.0	17.4
61	22.702	30.233	2.169	-82.3	-100	-16	0.30	2	2	c	130	160	144	0.583	15	4.4	0.64	2.5	9.8
62	22.704	30.479	1.796	-19.5	-207	11	0.33	2	1	c	90	170	124	0.848	5	5.5	0.38	0.9	2.0
63	22.708	30.240	2.071	-80.2	-112	12	0.38	2	2	c	150	150	150	0.000	45	6.1	0.48	2.1	5.4
64	22.708	30.139	3.376	-69.2	-113	14	0.34	2	2	c	120	270	180	0.896	-10	6.3	0.73	5.6	18.9
65	22.711	30.555	2.642	-34.1	-230	-12	0.46	2	1	p	230	250	240	0.392	-75	9.8	0.44	7.9	21.1
66	22.713	30.474	1.590	-21.8	-211	11	0.43	1	2	p	140	150	145	0.359	-65	6.5	0.44	1.7	3.9
67	22.713	30.186	2.775	-70.7	-117	7	0.45	1	3	c	230	380	296	0.796	-15	20.7	0.76	25.4	34.9
68	22.716	30.504	1.894	-29.5	-224	11	0.33	2	2	c	130	170	149	0.644	-45	6.6	0.32	1.3	2.9
69	22.718	30.837	6.379	-46.8	-248	20	0.43	2	1	c	200	270	232	0.672	-20	5.7	0.57	9.3	51.9
70	22.719	30.454	1.236	-18.6	-210	17	0.39	2	1	c	150	200	173	0.661	0	5.0	0.25	1.7	6.7
71	22.720	30.347	0.840	71.7	-135	21	0.36	2	3	c	170	300	226	0.824	25	5.3	0.53	7.9	47.1
72	22.721	30.112	3.801	-63.7	-113	8	0.36	3	2	c	210	360	275	0.812	-10	16.8	0.51	13.6	21.3
73	22.727	30.585	2.832	-41.8	-240	13	0.41	3	1	c	140	290	201	0.876	0	7.6	0.32	3.4	9.4
74	22.729	30.733	4.830	-47.2	-244	8	0.43	1	3	p	800	1250	1000	0.768	-35	61.3	0.44	574.5	1031.5

Column (6): Radial heliocentric velocity of maximum contrast. This value is accurate to the separation of the individual channel maps, 4.1 km s^{-1}.

Column (7): Expansion velocity, DV, (see text) to an accuracy of 2 km s^{-1}.

Column (8): Hole contrast defined as: contr $=(I_{surr}-I_{50}\%)/I_{surr}$. Errors of order 25% may occur.

Column (9): Type; see text.

Column (10): Quality of detection. This code gives the number -1 of the selection criteria met for the hole.

Column (11): Classification code, holes that show a clear elliptical shape over more than 90% of the outline are defined complete "c". Otherwise they are defined partial "p".

Column (12): and (13) Extent of the major and minor axis of the ellipse that can be fitted to the 50% intensity contour of a hole, in pc. Determination of these axes is accurate to 40 pc.

Column (14): Diameter of the hole as defined by the square root of the product of major and minor axis, in pc.

Column (15): Eccentricity of the hole to an accuracy of better than 0.08.

Column (16): Position angle of the major axis of the ellipse fitted to the hole. The angle is defined positive from the equatorial north pole in the anti-clockwise direction. The accuracy is of order 10°, but depends strongly on the ellipticity.

Column (17): Kinematic age assuming a constant expansion velocity. This is an upper limit to the true age. Errors may be of order 30%.

Column (18): Ambient density derived from the observed total column densities for the H I material surrounding the hole. A geometric correction is applied to correct for the inclination of M 33. The inaccuracies in the determination depend on the morphological characteristics of the surroundings and may be as high as 50%.

Column (19): Indicative mass assuming that the ambient density of column (18) equals the pre-hole density, and that the hole is spherically symmetrical. Propagation of error in the input parameter results in 50% deviations.

Column (20): Energy needed to create the hole. Propagation of errors in the input parameters results in 30% deviations.

Figure 2 shows the spatial distribution and sizes of the holes listed in Table 1.

Table 1 (continued)

no.	$\alpha_{(1950)}$ deg	$\delta_{(1950)}$ deg	R kpc	Θ deg	V_{cen} km s^{-1}	DV km s^{-1}	Cont.	T	Q	C	Major pc	Minor pc	Diam pc	ε	p.a. deg	Age 10^6 yr	n_{HI} at cm^{-3}	Mass 10^4 $M_\odot$	Energy 10^{50} ergs
75	22.730	30.414	0.629	0.4	-179	-20	0.41	2	1	c	70	130	95	0.843	-5	2.3	0.38	0.4	2.0
76	22.734	30.434	0.748	-18.3	-200	8	0.30	1	1	c	150	170	160	0.471	0	9.8	0.44	2.3	3.4
77	22.750	30.173	3.140	-55.6	-121	10	0.45	1	1	c	500	1000	707	0.866	-25	34.7	0.34	156.7	357.5
78	22.754	30.499	1.338	-51.4	-232	8	0.33	1	1	c	160	250	200	0.768	5	12.3	0.34	3.5	5.1
79	22.756	30.323	1.107	-54.2	-137	-11	0.23	2	2	c	70	120	92	0.812	-15	4.1	0.78	0.8	1.8
80	22.757	30.291	1.570	-52.8	-129	27	0.30	2	2	c	70	160	106	0.899	30	1.9	0.64	1.0	7.7
81	22.759	30.386	0.273	-42.3	-160	10	0.45	1	2	p	150	280	205	0.844	35	10.0	0.60	6.6	14.0
82	22.760	30.680	3.804	-54.4	-248	8	0.25	1	1	c	70	130	95	0.843	-10	5.8	0.37	0.4	0.5
83	22.760	30.254	2.102	-51.7	-113	-15	0.36	2	2	c	100	220	148	0.891	10	4.8	0.38	1.6	5.4
84	22.762	30.796	5.391	-54.5	-253	7	0.26	1	1	p	310	470	382	0.752	15	26.7	0.42	30.1	39.7
85	22.764	30.649	3.342	-55.9	-248	10	0.25	1	1	c	120	250	173	0.877	0	8.5	0.32	2.1	4.1
86	22.766	30.337	1.022	-42.8	-146	8	0.45	3	3	c	100	170	130	0.809	10	8.0	0.44	1.3	1.8
87	22.771	30.077	4.657	-50.1	-121	19	0.45	2	1	p	700	1150	897	0.793	-65	23.1	0.25	237.1	1319.0
88	22.773	30.422	0.337	57.0	-199	-16	0.36	2	1	c	100	160	126	0.781	-20	3.9	0.44	1.2	4.3
89	22.774	30.474	0.884	-75.7	-220	9	0.41	3	2	c	70	140	99	0.866	-5	5.4	0.32	0.4	0.6
90	22.775	30.407	0.372	19.5	-191	7	0.36	1	1	c	80	120	98	0.745	30	6.9	0.44	0.5	0.6
91	22.778	30.211	2.877	-45.3	-133	11	0.39	3	1	c	110	190	145	0.815	-5	6.4	0.60	2.3	5.4
92	22.779	30.382	0.650	-12.7	-180	28	0.43	2	1	c	100	170	130	0.809	0	2.3	0.44	1.3	10.3
93	22.782	30.307	1.627	-36.3	-142	13	0.46	2	2	p	120	170	143	0.708	10	5.4	0.57	2.2	6.2
94	22.782	30.322	1.439	-33.6	-142	-16	0.46	2	2	c	170	200	184	0.527	80	5.6	0.51	4.1	16.2
95	22.783	30.492	1.117	-80.0	-228	9	0.45	1	1	c	250	500	354	0.866	-25	19.3	0.25	14.5	25.4
96	22.787	30.418	0.585	30.7	-199	9	0.23	1	1	c	80	140	106	0.821	5	5.8	0.42	0.6	1.0
97	22.788	30.393	0.737	1.6	-187	7	0.39	1	3	c	150	180	164	0.553	0	11.5	0.51	2.9	3.5
98	22.793	30.336	1.436	-24.4	-146	16	0.34	2	3	c	130	170	149	0.644	-80	4.6	0.57	2.4	9.4
99	22.796	30.408	0.800	16.7	-199	11	0.43	1	1	c	140	190	163	0.676	-35	7.3	0.44	2.5	5.6
100	22.797	30.584	2.290	-73.1	-252	15	0.45	3	2	c	140	220	175	0.771	20	5.7	0.32	2.2	7.5
101	22.800	30.237	2.809	-36.2	-130	11	0.43	2	2	c	290	350	319	0.560	55	14.2	0.44	18.6	45.4
102	22.800	30.453	0.879	57.5	-224	14	0.43	1	2	c	320	500	400	0.768	15	14.0	0.32	26.3	88.8
103	22.800	30.775	4.835	-63.4	-257	-12	0.36	2	2	c	300	550	406	0.838	-20	16.6	0.32	27.5	75.1
104	22.803	30.482	1.127	74.2	-228	-11	0.28	2	1	c	70	110	88	0.771	20	3.9	0.15	0.1	0.2
105	22.804	30.203	3.316	-37.5	-129	10	0.43	3	3	c	140	250	187	0.828	5	9.2	0.60	5.1	10.5
106	22.810	30.501	1.352	77.8	-236	16	0.43	1	2	c	180	220	199	0.575	40	6.1	0.32	3.2	12.1
107	22.815	30.406	1.215	13.5	-203	6	0.23	1	1	c	120	180	147	0.745	-40	12.0	0.25	1.0	0.9
108	22.819	30.476	1.274	57.8	-228	11	0.43	1	1	p	170	260	210	0.757	-15	9.4	0.25	3.1	6.6
109	22.824	30.776	4.762	-69.2	-265	7	0.33	1	2	p	160	230	192	0.718	-40	13.4	0.63	5.8	7.4
110	22.827	30.453	1.347	39.7	-216	-20	0.38	2	2	c	150	190	169	0.614	40	4.1	0.44	2.8	14.5
111	22.839	30.538	1.957	72.8	-249	-16	0.45	2	1	c	140	190	163	0.676	30	5.0	0.76	4.3	17.4

2.2. *Characteristics of the H I hole distribution*

The final catalogue consists of 148 holes. We examine here the characteristics of the H I hole distribution in M 33, by determining relations among the observed and derived parameters. Distribution characteristics for each of the derived parameters are examined separately. Correlations between parameters are derived by examining scatter diagrams.

2.2.1. Distribution properties of each parameter

The radial distribution of the number of holes shown in Fig. 3 resembles the radial distribution of surface density in M 33 (see Fig. 10 of Deul and van der Hulst, 1986), but the number of holes decreases more rapidly at the larger galactic distances than the surface density. This is caused by two effects. First, warping of the outer H I layer of M 33 causes us to progressively miss holes at galactic radii beyond 5 kpc. Secondly, the parts where we should find holes at large galactic distances (i.e. the extreme ends of the major axis) are heavily attenuated by the combined primary beam of the H I survey. The H I hole survey, however, is relatively complete inside 5 kpc, and resembles the fragmentary spiral structure. The peak at 1.25 kpc coincides with regions of higher H I density around the southern spiral arm. Peaks around 3.25 and 4.25 kpc may represent other spiral arm segments. The decrease in the number of holes toward the center of M 33 follows the lack of H I emission within 1 kpc.

The distribution of hole diameters resembles an exponential increase of the number of holes with decreasing diameter. An extrapolation of the exponential fit to the diameter distribution, suggests that we have detected only half the expected number of holes, if we integrate the fit down to the resolution limit of the H I survey. The sharp cutoff below 125 pc indicates both our reluctance to include holes with diameters close to the beam size, and the intrinsic resolution cutoff: no holes smaller than 80 pc are included in the catalogue.

Examination of the distribution of the absolute value of the expansion velocities shows that the majority of the holes have expansion velocities around 15 km s^{-1}, but there is also a minor additional peak at 20 km s^{-1}. This can be traced back to the difference between Type 2 and Type 3 holes. The peak near 20 km s^{-1} is primarily due to Type 2 holes (dashed histogram in Fig. 3), while the peak around 15 km s^{-1} is caused by the combined distribution of Type 2 and 3 holes. However, for Type 2 our estimates are upper limits and the true values may be smaller (up to 60%) depending on the geometry of a particular hole. The velocity resolution limits the determination of DV to values greater than 4 km s^{-1}.

Table 1 (continued)

no.	$\alpha_{(1950)}$ deg	$\delta_{(1950)}$ deg	R kpc	Θ deg	V_{cen} km s^{-1}	DV km s^{-1}	Cont.	T	Q	C	Major pc	Minor pc	Diam pc	ε	p.a. deg	Age 10^6 yr	n_{HI} at cm^{-3}	Mass 10^4 $M_\odot$	Energy 10^{50} ergs
112	22.845	30.384	1.986	5.1	-199	9	0.30	2	1	c	90	140	112	0.766	5	6.1	0.09	0.2	0.2
113	22.845	30.580	2.383	81.2	-253	-16	0.18	2	1	p	400	600	490	0.745	85	15.0	0.32	48.2	201.6
114	22.846	30.321	2.571	-11.6	-162	11	0.33	3	1	c	120	200	155	0.800	50	6.9	0.19	0.9	1.9
115	22.848	30.516	1.904	60.6	-236	-18	0.33	2	1	c	70	110	88	0.771	0	2.4	0.09	0.1	0.3
116	22.855	30.608	2.742	83.1	-257	-18	0.38	2	3	c	120	180	147	0.745	20	4.0	0.51	2.1	9.4
117	22.860	30.282	3.253	-15.9	-154	12	0.47	2	2	c	380	600	477	0.774	25	19.5	0.19	26.8	70.2
118	22.864	30.492	2.068	44.9	-236	8	0.43	1	2	c	170	350	244	0.874	-10	14.9	0.25	4.8	6.8
119	22.865	30.656	3.292	87.7	-236	8	0.43	1	2	c	170	350	244	0.874	-10	14.9	0.25	4.8	6.8
120	22.867	30.190	4.435	-25.1	-261	10	0.33	1	2	c	100	130	114	0.639	25	5.6	0.38	0.7	1.4
121	22.871	30.675	3.535	88.5	-261	-12	0.43	2	1	p	100	160	126	0.781	15	5.2	0.32	0.8	2.0
122	22.875	30.344	2.911	-2.6	-183	19	0.41	2	1	p	70	120	92	0.812	10	2.4	0.42	0.4	1.9
123	22.891	30.382	2.957	7.1	-195	18	0.41	2	2	p	180	300	232	0.800	15	6.3	0.42	6.8	31.7
124	22.902	30.299	3.881	-7.6	-162	15	0.23	2	1	c	90	150	116	0.800	-20	3.8	0.51	1.0	3.5
125	22.917	30.418	3.276	15.5	-207	12	0.43	1	2	c	180	300	232	0.800	-30	9.5	0.25	4.1	10.2
126	22.927	30.280	4.540	-7.8	-154	-16	0.43	2	2	p	600	1200	849	0.866	-25	26.0	0.38	300.8	1372.1
127	22.930	30.533	3.327	41.9	-245	21	0.36	2	3	c	100	140	118	0.700	-25	2.8	0.63	1.4	7.6
128	22.930	30.661	3.913	68.6	-261	8	0.46	1	2	c	450	630	532	0.700	-10	32.6	0.51	99.1	167.7
129	22.934	30.869	5.977	-87.9	-269	10	0.26	1	1	c	200	300	245	0.745	-20	12.0	0.57	10.9	23.2
130	22.947	30.465	3.726	24.4	-207	-11	0.33	2	1	c	110	200	148	0.835	-40	6.6	0.38	1.6	3.5
131	22.965	30.706	4.648	67.6	-265	20	0.45	2	1	c	250	300	274	0.553	40	6.7	0.19	5.1	25.3
132	22.966	30.540	4.000	37.9	-245	-9	0.14	2	1	c	70	110	88	0.771	-10	4.8	0.29	0.3	0.4
133	22.968	30.480	4.116	26.0	-220	19	0.41	1	1	p	240	560	367	0.904	-5	9.5	0.32	20.2	103.8
134	22.979	30.612	4.362	49.6	-249	8	0.43	1	1	p	120	180	147	0.745	-10	9.0	0.19	0.8	1.0
135	22.983	30.777	5.406	73.3	-265	8	0.38	1	2	c	190	220	204	0.504	50	12.5	0.25	2.8	3.9
136	22.987	30.473	4.504	23.6	-220	8	0.41	1	1	c	130	220	169	0.807	25	10.4	0.25	1.6	2.2
137	22.989	30.506	4.468	29.2	-228	4	0.41	1	2	p	650	1000	806	0.760	-45	98.8	0.38	258.0	168.0
138	22.991	30.342	5.305	4.0	-183	7	0.45	1	2	c	550	900	704	0.792	40	49.3	0.38	171.5	240.4
139	23.002	30.830	6.035	75.7	-265	6	0.26	1	1	c	250	400	316	0.781	30	25.8	0.44	18.2	19.0
140	23.007	30.420	5.143	14.6	-195	-12	0.41	2	1	c	90	240	147	0.927	0	6.0	0.32	1.3	3.1
141	23.013	30.931	7.074	82.9	-277	4	0.20	1	1	p	330	400	363	0.565	90	44.5	0.32	19.7	11.4
142	23.024	30.628	5.171	45.6	-240	5	0.45	1	2	c	300	320	310	0.348	-70	30.4	0.25	9.8	7.4
143	23.032	30.548	5.274	32.7	-224	23	0.32	2	1	c	90	170	124	0.848	15	2.6	0.32	0.8	4.6
144	23.066	30.404	6.466	12.4	-195	-18	0.26	2	2	c	230	240	235	0.286	80	6.4	0.19	3.2	13.5
145	23.065	30.553	5.923	31.0	-228	5	0.23	1	1	c	300	600	424	0.866	20	41.6	0.13	12.5	9.0
146	23.076	30.596	6.097	35.9	-232	-12	0.26	2	1	c	150	300	212	0.866	20	8.7	0.32	3.9	9.9
147	23.081	30.758	6.546	55.6	-253	-12	0.20	2	1	c	420	730	554	0.818	10	22.6	0.13	27.9	70.7
148	22.543	30.334	4.171	24.5	-142	8	0.39	1	1	c	50	90	67	0.831	10	4.1	0.63	0.2	0.3

The distribution of the contrast parameter presented in Fig. 3 shows that the majority of the holes have a high contrast (around 0.45) and that there are few low contrast H I holes. Because selection criterion (iii) limits the recognition of candidate holes to high contrast objects, this is not surprising. The cutoff for contrast values larger than 0.5 is intrinsic to the definition of this value (see column 8 text).

We find a significant deviation from circular symmetry for the H I holes in M 33. The median eccentricity is of order 0.78. For the larger holes the eccentricity decreases. Holes with diameters larger than 500 pc extend well outside the denser parts of the disk of M 33. If we assume the z distribution to have an exponential scale height with, a FWHM of 100 pc, these larger holes extend out to relative densities of 10% or less. In such cases we may approximate the morphology of the hole, in the denser parts of the disk, by cylindrical symmetry. Because of the inclination of M 33 ($i=57°$; Deul and van der Hulst, 1986) we expect that the eccentricities of the larger holes (dotted histogram in Fig. 3), and the position angles of their major axes are similar to the value found for the disk of M 33, i.e. an eccentricity of 0.77. We indeed find that the position angles of the larger holes are aligned with the position angle of the disk of M 33. Thus, the majority of the larger holes appear to be indeed circular objects with little effect from shear. The smaller holes, which have in general a larger eccentricity and randomly distributed position angles, are intrinsically elliptical in shape.

The distribution of the kinematic age of a hole shows that the H I hole phenomenon takes place over a short time span. Most of the holes have an age younger than 7 10^6 yr, with only a few dozen at longer periods. This time scale is similar to the life times of massive stars of type O and B.

The mass swept out of a H I hole, assuming that the observed density of H I outside the hole equals that of the density of the interstellar medium prior to hole production, shows a maximum near 5 10^4 $M_\odot$.

For the energy distribution we note that the majority of the holes have formation energies around 10^{51} erg, which is appropriate for Type II supernova explosions as well as for stellar wind blown cavities. There are, however, a fair number of holes that represent energies up to 10^{54} erg. These larger holes cannot have been created by a single event so that other processes must be involved in the creation of these, predominantly, large holes.

2.2.2. Cross correlations

To investigate the relation between parameters we have made correlation diagrams for all permutations. Here we comment on the correlations found that follow from the selection criteria or

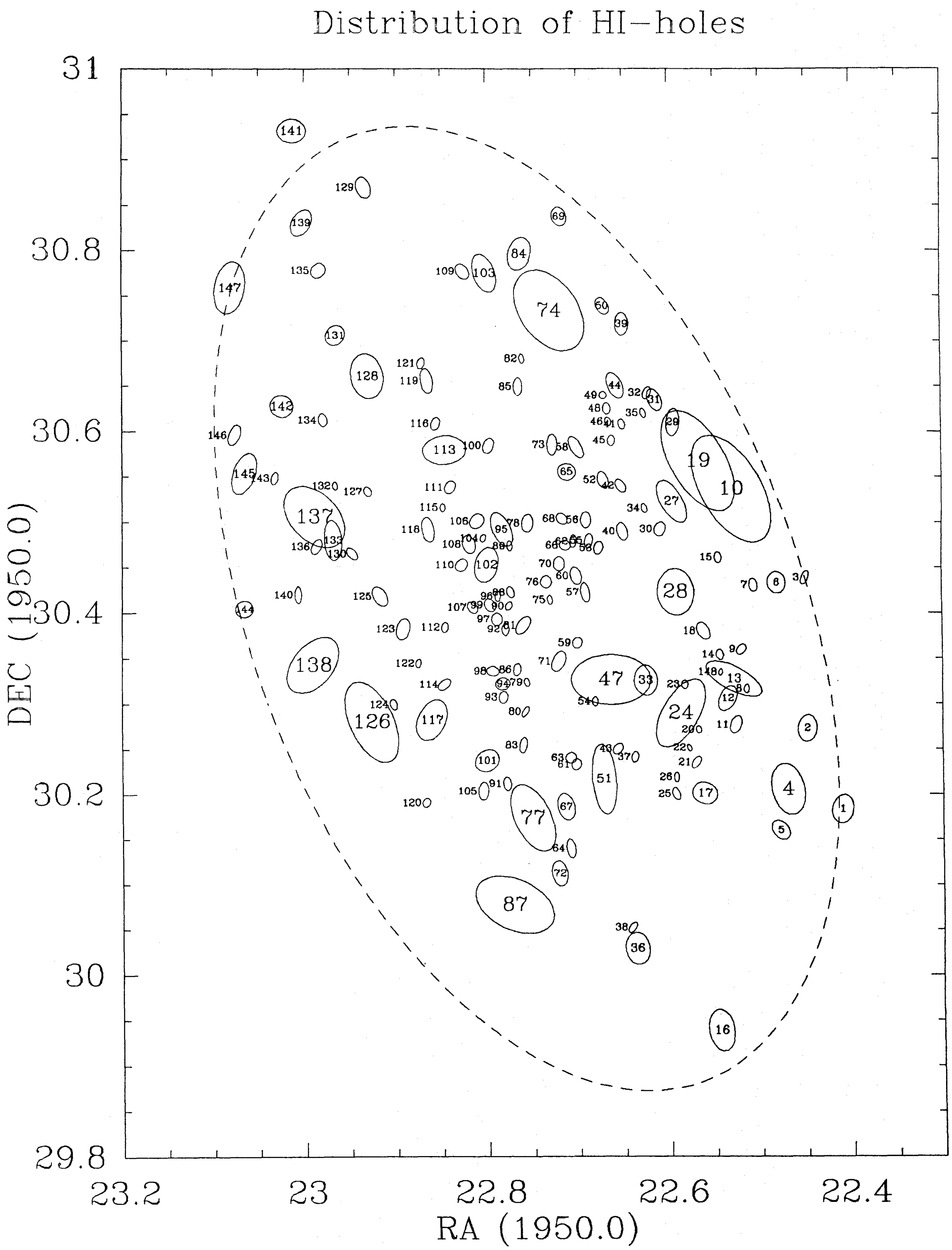

Fig. 2. Spatial distribution of the H I holes in M 33. Ellipses fitted to the H I survey are plotted in equatorial coordinates. The numbers correspond to Table 1. Note the concentration of small holes in the inner galaxy. The large holes are generally interarm cavities. The dotted ellipse outlines the region over which H I holes were searched

the definition of the parameters. We first concentrate on the quality, Q, type, T, and class, C, of the H I holes.

The quality of a hole depends on the density of the surrounding material, the contrast parameter, and to a minor extent on the diameter of the hole. These correlations are shown in Fig. 4. The mean of the distribution for each quality rating is given by the square; the error reflect standard deviation. For higher quality holes the density of the surrounding material is higher, the contrast is higher, and the diameter is larger. Because at higher densities of the surrounding material the chance of finding a hole with a complete and/or well defined circumference is higher, the quality rating is expected to be higher. The contrast between the

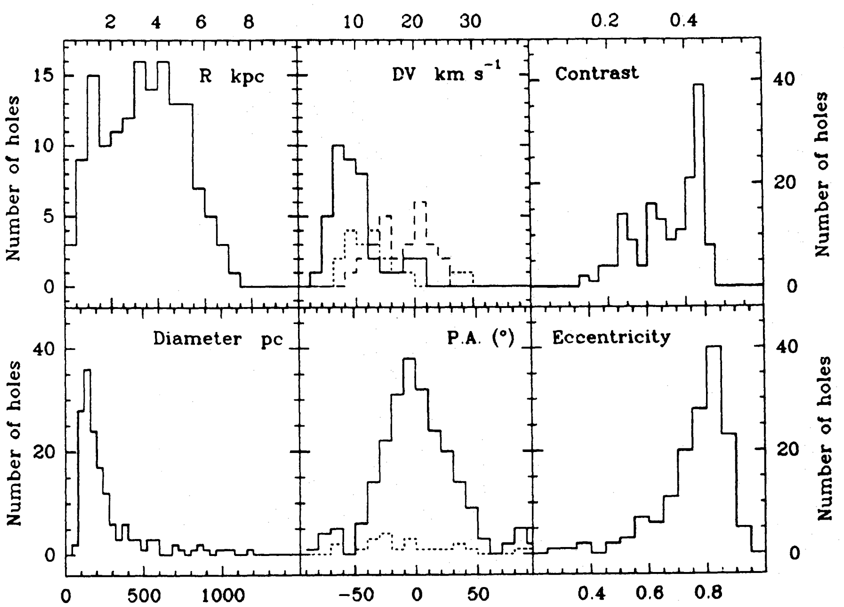

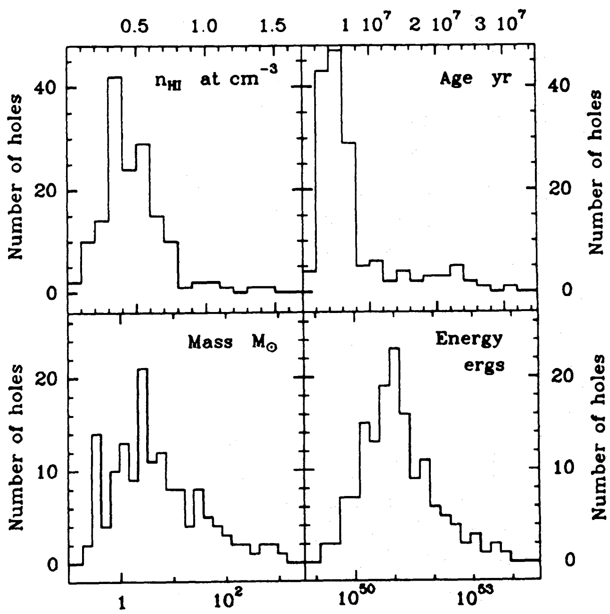

Fig. 3. Distribution properties of the H I hole catalogue. The panel showing the number of holes as a function of the DV parameter contains three separate curves. The full-drawn histogram represents the distribution of Type 1 holes; the dotted and dashed histograms that for Type 2 and 3, respectively. The panel showing the number of holes as a function of the position angle of a hole contains two histograms. The full-drawn line represents the distribution of all H I holes; the dashed one that of the large H I holes only. Both panels showing the number of holes as a function of mass and energy have the abcissa in logarithmic scaling

surrounding material and that inside the hole is, indeed, one of the selection criteria. The quality parameter depends only slightly on the hole diameter, with higher qualities for larger holes. The larger holes generally are better observable in the total column-density map, which was one of the criteria embedded in the quality rating. Because the larger holes tend to be only partially visible in a single channel map and because it takes several channels to embrace the outline of these holes, they are more difficult to recognize than holes that appear closed in consecutive channels.

The type parameter shows a correlation with the expansion velocity, the hole diameter, and the eccentricity of the hole. Figure 4 shows these correlations. From Type 1 to Type 3 holes, the diameter decreases and the eccentricity increases. This can be understood by the fact that the larger holes extend to large z distances; they generally have evolved out of the H I layer, causing the absence of H I emission over at least a large fraction of the velocity range. As we have seen in the previous paragraph there is an intrinsic relation between the hole diameter and its eccentricity. The expansion velocity of a hole is difficult to estimate for Type 2 holes, because only one side of the expanding shell is observable and we have to estimate, from the position-velocity diagrams, the central velocity of such holes. Figure 4 indicates that we have generally overestimated the expansion velocity with respect to the Type 3 holes, for which both red and blue-shifted H I is observable.

We have examined the radial behaviour of the following parameters: DV, contrast, eccentricity, diameter, $n_{\rm H\,I}$, age, mass, and energy. This was done by grouping the radii into bins and plotting the mean and standard deviation for each bin. Only for the diameter of a H I hole we find a positive correlation, with an increase in diameter at larger galactic radii. This effect is caused by the identification of larger holes (diameter $D > 500$ pc) that lie in the outer parts of M 33 between the spiral arms. For the smaller holes ($D < 500$ pc) there is a clear trend toward larger diameters at galactic radii larger than 5 kpc. It is at these galactic distances that the H I column density of the disk of M 33 starts to decrease, which facilitates expansion.

Examining the correlation for permutations among the parameters we find a correlation between the contrast of a hole and its diameter. The larger holes have generally higher contrast ratios than the smaller holes. This can be understood by examining the recognition procedure of H I holes. A small hole, which is generally complete, shows a better defined geometry than the larger holes, whose borders are only partially outlined by more dense H I material. For these larger holes to be identified as a hole the contrast between the average density in the hole and that of the surrounding material must be high enough to recognize the hole structure.

As was indicated before, the eccentricity of a H I hole is dependent on the hole diameter, such that the larger holes obtain axial ratios similar to that of the disk of M 33. The average position angle for the larger holes indeed aligns with the position angle of the disk of M 33. This is shown in Fig. 4 by the dashed histogram. The remaining combinations of the properties of the H I holes revealed no further intrinsic correlation.

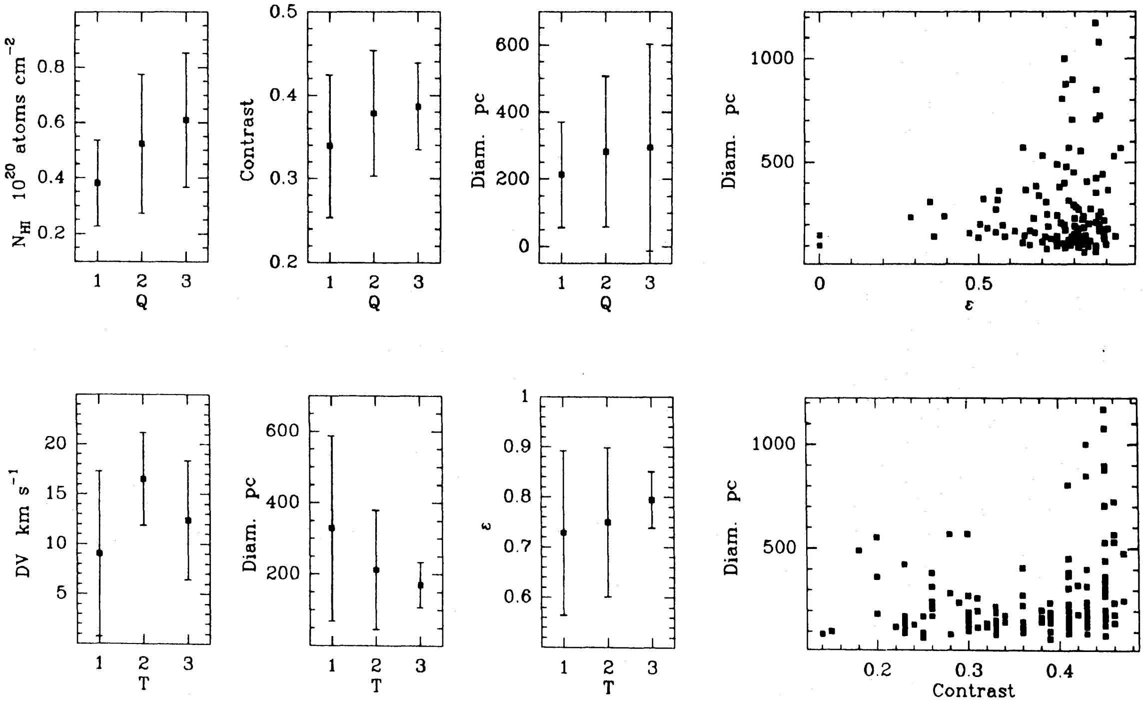

Fig. 4. Cross correlation among the parameters for the H I hole catalogue. Error bars are the standard deviations derived for the distribution per quality, Q, or Type, T, value. The scatter diagrams record the individual values for each hole in the catalogue

3. Correlation with other objects

Narrowing the types of objects down because the majority of theories on the origin of interstellar cavities are based on stellar winds and supernova scenarios, we searched for morphological correlations between the H I holes and the H II regions, OB association, candidate supernova remnant, and Wolf-Rayet star populations. The lists we obtained contain information on the position, the size and some special characteristics noted by the authors that published these catalogues.

The H II regions are taken from Courtès et al. (1987). Their classification of the 748 discrete H II regions (including new positions on 369 H II regions from Boulesteix et al., 1974) allows separation into three categories; diffuse emission (notably diffuse, diffuse halo, diffuse arc, diffuse ring or diffuse extension); dense H II regions (starlike, core, knot or multicore); and ring shaped (ringlike, bubble, arc, filament or loop). The H II regions without a remark of the sort just mentioned are designated 'normal'. We added to this list the classification of radio H II regions from Viallefond et al. (1986). For OB associations we used information from Humphreys and Sandage (1980); the size of the 143 OB associations listed was estimated from the plates given.

A list of supernova candidates and supernova remnant candidates was compiled from several papers (D'Odorico et al., 1978; Sabbadin, 1978; Sabbadin and Bianchini, 1979; Sabbadin, 1979; D'Odorico et al., 1980; and D'Odorico et al., 1982) to a total number of 39. The sizes of these remnants are negligible compared to the resolution limit of the H I survey. Wolf-Rayet stars were taken from Massey and Conti (1983).

The catalogue of H I holes was subdivided according to the properties of the hole distribution. This procedure allows investigation of the correlations between a particular class of H I holes and other objects. We divided the H I hole catalogue into the three Types, into low ($E < 2\,10^{51}$ erg), medium ($2\,10^{51}$ erg $< E < 5\,10^{52}$ erg), and high ($E > 5\,10^{52}$ erg) energies, into young (age $< 10^7$ yr) and old (age $> 10^7$ yr) ages, into small ($D < 200$ pc), medium (200 pc $< D <$ 500 pc), and large ($D > 500$ pc) diameters, and into low (contrast < 0.35) and high (contrast > 0.35) contrast.

3.1. Correlation methods

To correlate the H I hole distribution with the other objects, we use three different statistical techniques to determine either the overlap between two distributions or the correlation distance. The correlation technique based on the overlap of two different distributions directly uses both the positional and size information available. This method makes use of the surface of overlap for both kinds of objects, defined by

$$O_{\rm overlap} = O_{\rm holes} \cap O_{\rm other}. \tag{1}$$

Two extreme cases can be identified. If the surface of the region of overlap between the two populations equals that of either one, the correlation for that population is 100%. However, if the other population occupies the entire disk of M 33 the correlation is trivial. We define the expectation value of the surface of overlap as

$$E(O_{\rm overlap}) = \frac{O_{\rm holes}\, O_{\rm other}}{O_{\rm M\,33}}, \tag{2}$$

where $O_{\rm M\,33}$ is the surface of the area which was used for the search of H I holes (radius ~ 7 kpc). The expectation value may be used to discriminate between true correlation and chance coincidence. Assuming that the positions of the objects in both populations are randomly distributed, the probability to find an overlap value other than the expected can be described by a Poisson distribution with a mean value of $E(O_{\rm overlap})$. Using Monte-Carlo modelling this allows verification of the hypothesis: the calculated value is the result of an intrinsic correlation between the two populations.

The second technique to determine the existence of a correlation between the H I holes and the other objects makes use of a two-point spatial correlation function, $\xi(r)$, where r is the distance between a H I hole and an object from the other population. In this method we do not incorporate the sizes of the objects, only positional information is retained. The probability of finding an object of the other population within the infinitesimal surface, dA, around a H I hole can be expressed as

$$P=\sigma_{\rm other}\,dA\,(1+\xi(r)), \tag{3}$$

where $\sigma_{\rm other}$ is the surface density of objects from the other population. The correlation function is then defined by

$$\xi(r)=\frac{N(r)}{2\pi r\,dr}\,\frac{O_{\rm M\,33}}{N_{\rm other}}\,\frac{1}{N_{\rm holes}}-1, \tag{4}$$

where $N(r)$ is the number of objects from the other population that lie in the ring of width dr, at distance r from a H I hole. $N_{\rm holes}$ and $N_{\rm other}$ are the total number of objects in the H I hole and other population catalogues. The correlation function is determined within the radial boundaries $r=0$ and $r=\langle r_{\rm holes}\rangle$, where $\langle r_{\rm holes}\rangle$ is the average distance for neighboring H I holes. To convert the observed angular distances to true spatial distances in the plane of M 33 we use the inclination and position angle by Deul and van der Hulst (1986). The interpretation of the shape of the correlation function can be illustrated by three simple cases. Consider a significant correlation between the two populations on scales less than $1/8\langle r_{\rm holes}\rangle$. A plot of $\xi(r)$ vs. r would then show a maximum near $r=0$, which decreases rapidly to lower values near $1/2\langle r_{\rm holes}\rangle$. In case of an anti-correlation the curve would show the opposite behaviour; a maximum near $1/2\langle r_{\rm holes}\rangle$ decreasing rapidly to lower values near $r=0$. If there is no significant correlation between the two populations, $\xi(r)$ will show no structure with r, being relatively flat throughout the full range of r and having a value around 0. To verify if a particular distribution shows correlation we compare the plots of $\xi(r)$ vs. r for the objects with an identical plot obtained from a random distribution of the same number of objects per population. To get an idea of the spread in $\xi(r)$ at each r we used a Monte-Carlo process to determine the mean value and standard deviation.

The last method we used is the percolation technique. It is built around the principle "my neighbor's neighbor is my neighbor". In fact the percolation technique is not so much based on the distance between two individual objects as on the effective distance in and between a group of objects, that not necessarily need to be of a similar physical type. Similar to the correlation technique the spatial distances are used rather than the angular ones. The percolation distance $R_{\rm perc}$ is exponentially scaled such that the step size is optimal for the expected clustering distance. This means that half of the total number of steps lie within the two distances $R_{\rm min}$ and $R_{\rm average}$, where $R_{\rm min}$ is the minimum distance between two member found in the group and $R_{\rm average}$ is the average distance between two members in the group. The remaining half of the total number of steps lie within the two distances $R_{\rm average}$ and $R_{\rm max}$, where $R_{\rm max}$ is the maximum distance found between two neighboring objects in the group. Shandarin and Zeldovich (1986) introduce a dimensionless parameter, B, as the mean number of objects in a particular volume. We use the two-dimensional version: $B=\pi R^2\langle n\rangle$, where $\langle n\rangle$ is the mean number of objects in the total surface. The critical value, $B_{\rm c}$, is defined as the point at which a considerable reduction in the number of groups occurs, so called percolation. A group is a set of objects (that need not necessarily of similar physical type) which are connected because the individual distance among the objects is less than the percolation distance. Estimation of $B_{\rm c}$ is accomplished by a function, $\chi(B)$, that uses the dependence on distance of the mean number of objects of all groups, except the largest one. The function is as follows:

$$\chi(B)=\frac{\sum_i' N_{\rm groups}(i)\,i^2}{\sum_i' N_{\rm groups}(i)\,i} \tag{5}$$

where $N_{\rm groups}(i)$ is the number of groups with i objects, and the primed sum indicates that the sum runs over all but the largest cluster. We can thus use the $\chi(B)$ function to estimate the $B_{\rm c}$ values for the distribution of a given sample of objects. The advantage of using the $\chi(B)$ function is that it not only gives the value of the distance at which percolation occurs on a sample wide scale, but it also peaks for distances were the number of clusters decreases dramatically, not necessarily down to one. In this way we obtain a measure for the overall correlation distances within a sample of objects. To establish whether a correlation exists between two populations, we must compare the plots of $\chi(B)$ vs. B of each population separately with a similar plot of the combined population. In principle each population will show peaks in $\chi(B)$ at different B values depending on the characteristics of the distribution for that population. If, however, we examine the $\chi(B)$ vs. B plot for the distribution of objects containing both populations, then the position of the first peak may occur at values of B much smaller than that for the separate populations.

Let us examine three simple cases. First assume that there is no correlation between the two populations of objects and that both have a Poisson distribution. The position at which $\chi(B)$ peaks should then be the same for the separate as well as for the combined groups. In such cases $B_{\rm c}$ has a value of 5.4. Secondly let us assume an anti-correlation between the two populations, both having a similar amount of objects. Here the values of B, where $\chi(B)$ peaks, may be widely different, because the objects of one population occupy the holes (e.g. large number of groups) left by the other population (e.g. network structure). If we determine the $\chi(B)$ peaks for the combined group of objects the value of B will be roughly identical to that of a Poisson distribution because the combined group will evenly fill the entire space with objects so that percolation on a sample wide scale occurs for a value of B similar to 5.4. Finally consider the case of correlation between the two populations. Determination of the peaks in the $\chi(B)$ function for the separate populations should, for both distributions, result in similar values of B. By using the combined distribution of both populations an additional peak, at a smaller value of B, should occur, indicating that there is an extra percolation distance for the combined group which is much smaller than that for the separate distributions. In fact, in this case, a group of objects would generally consist of two objects, one of each population. An important advantage of this technique is that intrinsic structure in the individual populations, such as concentration in spiral arms, which may cause faulty identification of correlation for the other two techniques, is irrelevant in this case.

3.2. Correlations found

For all permutations among the sub-groups in the H I hole catalogue, the H II region catalogue and the main groups of OB associations, supernova remnants and Wolf-Rayet stars, we plotted the correlation function vs. the correlation distance. Plots that showed significant signs of (anti)correlation were re-examined by incorporating the possible errors in the correlation function via Monte-Carlo simulation of the particular populations under examination. We found that in many occasions the correlation, first thought to be significant, could be explained by low number statistics. The correlations that were found are discussed here. Note the absence of the H II subgroups: ring shaped and diffuse emission. These subgroups showed no correlation with the H I holes or its subgroups and consequently were left out further discussion.

We discuss here some of the correlations found. Both the positions of the H II regions and OB associations are correlated with those of the H I holes. After examination of the shape of the correlation functions, the H II regions show a correlation over a much wider distance range than the OB associations. The half power width of the correlation function for the H II regions is 250 pc, indicating that the majority of the H II regions lie within this distance interval from the H I holes. The expected correlation distance, however, is 350 pc, which makes the correlation marginally. Because the mean diameter of the H I holes is 150 pc a large fraction of the H II regions may be positioned outside the H I holes. The half power width of the correlation function for the OB associations is much smaller, <100 pc, indicating the most of the OB associations lie within the boundaries of the H I holes. The expected correlation distance (half power width) is 400 pc, so that we may accept the hypothesis of correlation. There are, however, a large number of uncorrelated objects that cause the correlation function to remain about a level of 0.7 for larger values of the distance (see Fig. 5). This is verified by the percolation analysis. The χ distribution for the separate groups of the H I holes and OB associations are quite similar (see Fig. 5), but the χ function of the combined population, shows around $B=1.2$ a peak which is not present in the χ functions for the separate populations. This suggests that the combined population (OB associations and H I holes) has a smaller percolation distance than the separate populations, meaning that the average distance (normalized to unit density) between individual OB associations and H I holes is smaller than the average distance within each individual group. Thus OB associations tend to cluster near H I holes.

The positions of the supernova remnants are not well correlated with those of the full catalogue of H I holes. If holes are caused by supernovae, then identified supernova remnants should, indeed, avoid holes. Assuming that the H I hole formation process is the result of the collective effects of stellar winds from stars in an OB association and the accompanying supernova explosions, a H I hole must have an age much older than the lifetimes over which supernova remnants are optically observable. The site where the supernova remnants are observed may be the position where future H I holes will be found. The correlation function for the Wolf-Rayet stars shows hints of a correlation on scales less than 200 pc. Again, the large distance, within which most of the correlation occurs, indicates that the positioning of the Wolf-Rayet stars is not preferentially inside the H I holes, but that they lie within a wide range of distances from the centers of H I holes. The percolation analysis shows that the combined population has no special characteristics other than those already present in the separate ones.

To verify whether the correlations found are dependent on a particular parameter of the H I hole distribution, we obtained identical plots for the correlation and percolation function of the subdivision as specified in Sect. 3.

The correlation found between the full catalogues of the H I hole and H II region distribution is also found in one ro more subgroups. The size of the H I holes is a parameter on which the correlations depends strongly. The small H I holes show better correlation with the full H II region catalogue. The overlap area for small H I holes is significantly larger than that for the other sizes; the correlation function has a half power width of order 200 pc, which is less than that for the full H I hole catalogue. Based on diameter arguments, one would expect a subset of the small H I holes to be correlated with the giant H II regions. In fact NGC 604, NGC 595 and IC 133 coincide with H I holes no. 127, no. 57, and no. 31, respectively. Their diameters and position angles correspond to those of the H II regions. The medium and large size H I holes show anti-correlation with the full H II region catalogue, such that the correlation function is small near distances of 0 pc but peaks near 300 pc and 550 pc, respectively. This anti-correlation effect for medium and large size holes causes the correlation function between the full catalogues of H I holes and H II regions to become more extended than that for the small holes alone. The percolation function for small, medium, and large holes confirms this situation. Particularly for the larger holes it is evident that H II regions occupy the area of M 33 outside the H I holes, with a tendency to cluster along the borders of these large holes. Principally all large H I holes are interarm regions and enclosed by spiral arm segments.

The class parameter is also a discriminator for good correlation between H I holes and H II regions. The complete holes tend to be correlated over the same distances ($\simeq 200$ pc) as the full H I hole catalogue, but the partial holes show indications of anti-correlation with a characteristic distance of order 500 pc. The anti-correlation hypothesis is not supported by the percolation plots, but for the complete holes the χ function shows an extra peak, at low B, not present in the separate populations. The relative overlap area for complete holes is almost four times larger than that for the partial holes, indicating that significantly more H II regions overlap with complete H I holes than with partial ones.

For the energy subgroup, the low energy holes show correlation with the full H II region catalogue as expected, because low energy holes are predominantly small in size. The correlation distance, again, in somewhat large and is identical to that for the full H I hole catalogue (250 pc). Again the expected half power width of 350 pc makes this correlation marginal. Continuing through medium energy holes the correlation breaks down such that at the high energy holes no correlation is found at all.

If we search for correlation characteristics of the subdivisions of the H I holes with the subdivisions of the H II regions catalogue, we find the following characteristics. Although the number of objects involved become significantly smaller, the Type 1 and 2 holes are best correlated with the 'normal' H II regions, while Type 3 only shows significant correlation with the 'dense' H II

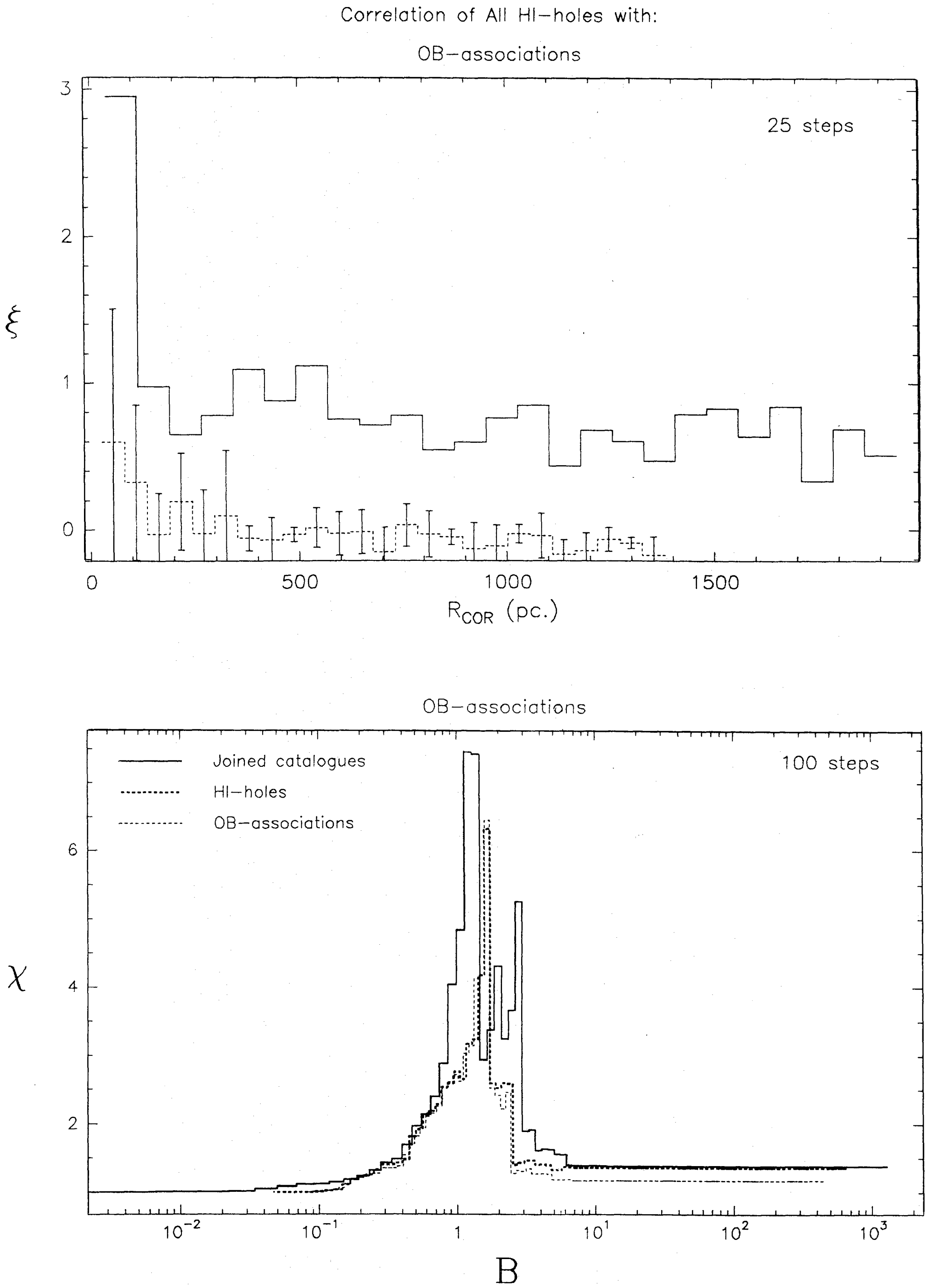

Fig. 5. Correlation and percolation functions for the full H I hole catalogue with the OB associations catalogue. For the correlation function the full drawn line shows the distribution of ξ as a function of distance; the dotted line represents the distribution of ξ for the same number of randomly distributed objects as in the combined population. The error bars are estimates of the errors, determined from the standard deviation obtained from six trial runs on random distributions. For the percolation function the full-drawn lines show the distribution of χ for the combined population as a function of the parameter B; the dotted and dashed lines represent the χ distribution for the H I holes and OB associations, respectively. Note the presence of a strong peak for the combined population at a B value less than those where the separate populations peak, indicating the existence of a smaller relative percolation distance for the combined population

regions. Both the correlation function and relative overlap areas support this view.

Correlation of the radio H II regions subgroup with the separate subgroups of the H I hole distribution shows characteristics similar to those found for the 'normal' H II regions. There are, however, some exceptions. The positions of radio H II regions do not coincide with those of medium or large holes, they are concentrated around the small H I holes with a peak in the correlation function near 150 pc. The relative overlap area of radio H II regions with large H I holes is zero! The correlation with low energy H I holes is much tighter (<110 pc, 250 pc expected) for radio H II regions than for 'normal' H II regions (<275 pc, 300 pc expected). The percolation analysis confirms this situation, because for the 'normal' H II regions the peak of the χ function lies in the network range of B values, while that for the radio H II regions lies near the cluster range. Again the relative overlap area for high energy H I holes is zero, indicating that the radio H II regions avoid high energy holes.

Checking for correlations between the OB association catalogue and the H I hole subgroups, we find that the OB associations tend to lie closer to the small H I holes. The correlation distance for this combination of populations is of order 100 pc. Although the percolation analysis also shows smaller percolation distances with the medium and large size holes, the correlation

Table 2. Overlap properties of the H I holes with respect to the H II regions and OB associations. The EM code is taken from the H II region catalogue of Boulesteix et al. (1974). The H I–H II, H I–OB, and H II–OB overlap codes are defined as follows: (1) 100% overlap (e.g. generally the H II regions lies within the H I hole), (2) between 100% and 50% overlap, (3) between 50% and no overlap

HI Hole no.	HII Region no.	EM Code	HI–HII Code	OB Assoc. no.	HI–OB Code	HII–OB Code
1	Z393		1			
4				125	2	
4				126	1	
4				127	3	
5	268	2	2			
5	270	2	3			
5	Z263		1			
6	Z 60		3	135	3	2
6	Z401		1			
7				135	3	
9	Z 69A		3	23	3	2
10	Z 58		1			
10	Z 90		1			
10				136	1	
11	240	2	3			
11	241	2	3			
11	Z 74		1			
11	Z 76		3			
13	231	2	1			
13	232	2	1			
13	233	2	2			
13	234	2	1			
13	235	2	3			
13	237	2	1			
13	Z 75		1			
13	Z 75A		2			
13				21	3	
13				22	1	
14				24	2	
17				124	1	
18	Z 79		3			
18				25	3	
19	618	3	1			
19	619	2	1			
19	620	2	1			
19	621	1	1			
19	Z 95		1			
19	Z 96		1			
19	Z 97		1			
19	Z101		2			
19	Z102		2			
19				136	3	
21	Z 27A		2			
22	Z 26A		3			
22				130	3	
23	Z114		2			
23				20	3	
24	226	3	2	130	2	3
24	215	2	1			
24	Z114		2			
24	Z115		2			
24	Z 116		3			
24	Z 117		1			
24	Z 123A		2			
24				19	1	
24				20	1	
24				21	3	
24				131	1	
25	220	3	2			
25	221	3	3			
27	Z 100		3			
28	285	2	2			
28	286	2	1			
28	Z 82		1			
28	Z 83		2			
28	Z 84		1			
28	Z 85		2			
30	Z 193		2			
30	Z 196		2			
30	Z 198		2			
31	623	3	2			
31	624	3	2			
31	625	2	2			
31	626	3	2			
31	Z 104A		1			
31				139	3	
32	Z 104A		3			
32				139	3	
33				18	3	
33				53	3	
34				30	3	
35				139	3	
36	254	2	1			
42	608	2	1			
47	1003	2	1	51	3	3
47	1004	2	1	52	1	2
47	Z 33A		3	14	3	3
47	Z 132		3	14	3	2
47	209	3	1			
47	210	3	1			
47	Z 131		1			
47	Z 133		3			
47				16	3	
47				18	3	
47				53	1	
47				54	3	
50	Z 285		2	141	3	3
52	609	2	2	31	2	2
54	209	3	2			
54	Z 132		3			
57	49	4	3	61	3	3
57	49	4	3	62	3	2

function and the overlap areas suggest that this might be the effect of the small number statistics involved. Correlations between the OB associations and the low energy H I holes again show distances in the range of 100 pc. In accordance with this situation there is also a positive correlation with the young H I holes, both suggested by the correlation and overlap analysis. There is, however, no tendency toward a specific H I hole type.

Due to the low number statistics involved in the correlation between Wolf-Rayet stars with the H I hole subgroups, we refrain from further analysis for these objects.

The percolation analysis shows that all distributions peak in the network domain of the $\chi(B)$ vs. B plot. This suggests that the interarm cavities play a dominant role in the distributions and confirms the hypothesis that most star formation takes place in spiral arm segments.

Table 2 is a cross reference table for the correlation between the H I holes and OB associations and H II region. This table records the overlap codes between the H I holes and the OB associations, between the H I holes and H II regions, and between the OB associations and H II regions corresponding to one hole.

Table 2 (continued)

HI Hole no.	HII Region no.	EM Code	HI–HII Code	OB Assoc. no.	HI–OB Code	HII–OB Code
57	Z 80		1			
58	629	3	3	33	2	2
60				62	3	
60				63	3	
65	Z 214		2	32	2	1
66	Z 213		3			
66				66	3	
68	612	2	3			
70	59	4	3			
71	1002	2	3	50	2	2
72	247	1	1	112	1	1
72	246	4	2			
72				114	3	
74	641	2	3	143	3	2
74	Z 286		1			
74				142	3	
77	Z 148A		3	110	2	3
78				68	2	
80				7	3	
81	9	3	1	144	2	2
82	637	2	3	140	3	2
83	Z 146		1			
83	Z 147		2			
86	10	3	2	3	2	3
87	Z 308		1	113	1	1
87	Z 309		1	113	1	1
87	Z 315		1			
91	Z 148A		2	109	3	2
92	73	3	3	145	2	3
92	96	3	1	145	2	1
93	707	3	3	4	3	1
93	707	3	3	5	3	2
94	11	3	2	4	2	2
94	Z 1A		3	2	3	3
94	Z 1A		3	4	2	2
94	Z 4A		3	2	3	1
95	301	4	3	69	3	1
95	758	2	1	69	3	2
95	758	2	1	70	3	3
95	Z 232		1	69	3	1
98	4	3	3	1	3	2
98	4	3	3	2	3	3
98	5	3	2	2	3	1
99	81	3	1			
100	675	3	3			
100				72	3	
101	Z 174		3			
101				108	3	
102	74	3	2			
102	Z 235		2			
102	Z 238		1			
102	Z240		1			
102				96	3	
103	Z291		1			
104	Z239		3			
104	Z242		2			
106	Z227		2	74	2	1
107				98	2	
109	Z306		2			
113	Z249		3			
113	Z251		1			
113	Z252		1			
113	Z259		1			
113	Z260		1			
113				79	3	
114	709	2	2			
114				103	2	
115	Z257		2			
115				81	3	
116	Z172		3	38	3	1
116	691		3			
116	Z271		3			
117	710	3	3			
117	Z187		3			
117	Z188		1			
117				104	3	
118	Z256		3			
118	Z277		3			
118				82	3	
119	660	1	3	41	2	3
121				41	3	
121				43	3	
125	734	3	1			
125				94	3	
125				99	2	
126	Z190		3			
126	Z353		1			
127	680	4	2			
128	Z374		3			
128				46	2	
131	Z383		2			
133	749	3	3			
133	750	3	1			
133	Z304		1			
137	749	3	3	88	3	3
137	750	3	3			
137	Z243		1			
137	Z304		2			
138	Z359		1			
138	Z360		2			

3.3. *Molecular origin*

As briefly mentioned, earlier, an entirely different explanation for the absence of H I emission could be the local conversion of atomic to molecular hydrogen. Thus, an H I hole would in fact represent an H_2 concentration. The mean column density of such an H_2 cloud (complex) should be at least equal to 0.5 times the 'missing' column density of H I $N_H \simeq 0.75\ 10^{21}$ atom cm^{-2}. Such a column density of H_2 is expected to be associated with an integrated CO signal of strength $I_{co} \simeq 2f(\mathrm{CO})$ K km s^{-1}; the numerical factor follows from the galactic ^{12}CO-to-H_2 conversion (Bloemen et al., 1986; Deul et al., 1988), whereas f(CO) represents a possible difference in the conversion factor for M 33. With $DV = 15$ km s^{-1}, and a mean hole size of 200 pc, we thus should find a CO signal of order 0.13f(CO) K in a 1′ beam. To verify this explanation, we have used the NRAO[1] 12-m Millimeter Radio Telescope (HPBW$\simeq$1.′1) to obtain ^{12}CO($J = 1 \rightarrow 0$) measurements of small, high-contrast H I holes (no. 34, no. 35, no. 99, no. 122). Taking into account the velocity width, the hole diameter relative to beam size, the ambient

[1] The NRAO is operated by Associated Universities, Inc., under contract with the U.S. National Service Foundation

column density and an efficiency of 75%, the expected CO signals are: $T_A^* = 0.096$ K, 0.033 K, 0.181 K, and 0.033 K. We observed both the center and 3–4 edge positions of each hole. No ^{12}CO emission was detected at any position above 60 mK ($3 \times$ rms value). Testing the hypothesis whether small, high-contrast holes are filled with molecular hydrogen, we may combine the results from the four holes and derive an average $N_{\rm H\,observed}/N_{\rm H\,expected} < 0.3\, f({\rm CO})^{-1}$. Thus, either $f({\rm CO}) < 0.3$, or the holes do not contain sufficient molecular hydrogen to consider the atomic to molecular hydrogen conversion an acceptable hypothesis.

In case of NGC 604, Israel et al. (1988) have detected H_2 ($1 \rightarrow 0$ Q-branch) emission indicating the presence of a large molecular cloud with mass of order $10^7\ M_\odot$. This molecular cloud has a morphology similar to the H I hole no. 127. By comparing their molecular mass estimate with the observed ^{12}CO line intensity (Blitz, 1985), Israel et al. (1988) derive $f({\rm CO}) < 0.3$, in agreement with our upper limit. So there are good indications that the ^{12}CO-to-H_2 conversion factor is less than the galactic value, but this still does not confirm the earlier posed hypothesis.

4. Discussion

As described above we have found (i) that the H I holes are best correlated with the OB associations and (ii) less well with the H II regions, but (iii) some small H I holes are correlated with large H II regions. (iv) We could not establish meaningful correlations for the Wolf-Rayet stars nor (v) for supernovae and their remnants. (vi) Examination of the ^{12}CO non-detections for small, high-contrast H I holes does not allow rejection of the hypothesis that H I holes are due to conversion of atomic hydrogen to the molecular state. We discuss here some of the implications suggested by these correlations, and in particular comment on the meaning of the correlations found between the separate subgroups of the H I holes with the other objects.

The OB associations show the closest positional correspondence with the H I holes. The preference of the OB associations for small H I holes may be understood in the following way. The sizes of the OB associations, as derived from the plates in the article by Humphreys and Sandage (1980) are less than 200 pc. If stellar winds are responsible for excavating the cavity in the H I layer of M 33, these holes may not be much larger than 200 pc in diameter, which is in fact the limit for the small H I hole subgroup. Similarly, the OB associations overlap significantly better with small diameter H I holes than with old and high energy holes, which are mainly due to larger holes. The cutoff in age at $7.5\,10^6$ yr is similar to the ages obtained for the OB associations by Humphreys and Sandage (1980).

The correlations found between the H I holes and the H II regions are less well defined than those for the OB associations. The H II regions tend to concentrate toward the boundaries of the large holes. This reflects the fact that these holes are principally interarm regions; the edges of the large holes are mainly formed by spiral arm segments in which we know star formation to take place. These large holes are all Type 1 holes, which indicates that there is little neutral atomic hydrogen present at these positions. A correlation exists between the H II regions identified as dense as well as the radio H II regions with the Type 3 holes. In particular three giant H II regions are positioned exactly on H I holes of similar diameter. The stars in these giant H II regions ionize the neutral atomic hydrogen in their surroundings, causing the absence of 21-cm line emission. It is unclear to what degree a small H I hole is due to the ionization effect from these giant H II regions or to the conversion of atomic hydrogen to molecular form.

The average energy for the H I hole ensemble is a few 10^{51} erg. If we assume that the H I holes are the result of supernova explosions only, a few tens to hundred Type II supernova events are necessary to power the excavation of the H I layer. Bruhweiler et al. (1980) and Brinks and Bajaja (1986) adopt a supernova rate of 10^2 per shell for the galactic supershells and H I holes in M 31, respectively. Using this value for the supernova rate per H I hole in M 33, we calculate, assuming a maximum age of $7\,10^6$ yr for the H I holes, a Type II supernova rate of 3 per 1000 years. This is about a factor of three lower than the supernova rate given by Tammann (1978) and Berkhuijsen (1983), but their value lies within the errors of our determination. This value of the supernova rate is similar to the local value found for the Galaxy. We do not, however, expect a correlation between the supernova remnants and H I holes because Type II supernovae generally occur inside a cavity excavated by stellar winds from the OB association. Therefore, there is no material left for excitation to a supernova remnant.

A small fraction of the interstellar medium in M 33 is filled by the holes. Because the identification of large holes was influenced by spiral-arm geometry, we should base the determination of the filling factor on the small and medium sized holes only. To determine an upper limit, however, we do include them and allow a factor of 2 for non-detected holes. The filling factor thus determined is $<40\%$ of the surface of M 33. If the H I holes are principally the result of Type II supernova explosions, the filling factor for hot low density gas would be no more than that of the H I holes, which is much smaller than the suggested 70–80% (McKee and Ostriker, 1977). Indeed, there is little sign of overlapping shells in M 33.

5. Conclusions

We assumed that the H I distribution in M 33 can be described as a H I layer with a large number of holes; then the following results are obtained.

A total of 148 holes is found (lower limit). Diameters range from 40 pc (the resolution limit of the H I survey of M 33; Deul and van der Hulst, 1986) and 1 kpc. The average hole diameter increases with increasing galactocentric distance and the largest holes are interarm cavities. From surrounding H I column densities we find the swept up mass to range from $10^3\ M_\odot$ to $10^5\ M_\odot$, with corresponding energies between 10^{49} erg and 10^{54} erg. Ages based on measured expansion velocities and diameter are of order 10^7 yr.

Using three statistical techniques (two-point correlation function, region of overlap, percolation) the positional correlation between H I holes and OB associations is shown to be tight, particularly for the smaller holes ($D < 200$ pc). The estimated ages for H I holes and OB associations are similar (Humphreys and Sandage, 1980). The correlation with H II regions is found to be less tight. Table 2 lists these correlations and their overlap codes. The three giant H II regions NGC 604, NGC 595, and IC 133 coincide with H I holes of similar diameter, suggesting that the ionization of the interstellar medium causes the absence of 21-cm line emission in such cases.

The non-detection of ^{12}CO emission for four small, high-contrast H I holes implies that either the conversion factor between ^{12}CO integrated intensities and molecular hydrogen column density is $<0.3\times$ the galactic conversion factor, or the amount of molecular material in these holes is smaller than that expected from the surrounding atomic column densities.

If the creation of H I holes is due to a combination of stellar winds and supernova explosions, then a supernova rate of order 3 per 1000 years is derived, which is (within the errors of determination) similar to those found by Tammann (1978) and Berkhuijsen (1983).

The filling factor of <40% for the H I holes in M 33, which is based on all holes allowing a scaling factor of 2 for non-detected holes, is smaller than the expected value as discussed by McKee and Ostriker (1977) for our Galaxy.

References

Berkhuijsen, E.M.: 1983, *Astron. Astrophys.* **120**, 147

Blitz, L.: 1985, *Astrophys. J.* **296**, 481

Bloemen, J.B.G.M., Strong, A.W., Blitz, L., Cohen, R.S., Dame, T.M., Grabelsky, D.A., Hermsen, W., Lebrun, F., Mayer-Hasselwander, H.A., Thaddeus, P.: 1986, *Astron. Astrophys.* **154**, 25

Boulesteix, J., Courtès, G., Laval, A., Monnet, G., Petit, H.: 1974, *Astron. Astrophys.* **37**, 33

Brinks, E., Bajaja, E.: 1986, *Astron. Astrophys.* **169**, 14

Bruhweiler, F.C., Gull, T.R., Kafatos, M., Sofia, S.: 1980, *Astrophys. J. Lett.* **238**, L27

Castor, J., McCray, R., Weaver, R.: 1975, *Astrophys. J. Lett.* **200**, L107

Chevalier, R.A.: 1977, *Ann. Rev. Astron. Astrophys.* **15**, 175

Courtès, G., Petit, H., Sivan, J.-P., Dodonov, S., Petit, M.: 1987, *Astron. Astrophys.* **174**, 28

Deul, E.R., Bloemen, J.B.G.M., Thaddeus, P.: 1989, *Astron. Astrophys.* (submitted)

Deul, E.R., van der Hulst, J.M.: 1986, *Astron. Astrophys. Suppl.* **67**, 509

D'Odorico, S., Benvenutti, P., Sabbadin, F.: 1978, *Astron. Astrophys.* **63**, 63

D'Odorico, S., Dopita, M.A., Bevenutti, P.: 1980, *Astron. Astrophys. Suppl.* **40**, 67

D'Odorico, S., Goss., W.M., Dopita, M.A.: 1982, *Monthly Notices Roy. Astron. Soc.* **198**, 1059

Elmegreen, B.G., Chiang, W.-H.: 1982, *Astrophys. J.* **253**, 666

Heiles, C.: 1979, *Astrophys. J.* **229**, 533

Heiles, C.: 1984, *Astrophys. J. Suppl.* **55**, 585

Hu, E.M.: 1981, *Astrophys. J.* **248**, 119

Humphreys, R.M., Sandage, A.: 1980, *Astrophys. J. Suppl.* **44**, 319

Israel, F.P., Hawarden, T.G., Wade, R., Geballe, T.R.: 1988, preprint

Massey, P., Conti, P.S.: 1983, *Astrophys. J.* **273**, 576

McCray, R., Kafatos, M.: 1987, *Astrophys. J.* **317**, 190

McKee, C.F., Ostriker, J.P.: 1977, *Astrophys. J.* **218**, 148

Meaburn, J.: 1980, *Monthly Notices Roy. Astron. Soc.* **192**, 365

Sabbadin, F.: 1978, *Publ. Astron. Soc. Pac.* **90**, 563

Sabbadin, F., Bianchini, A.: 1979, *Publ. Astron. Soc. Pac.* **91**, 62

Sabbadin, F.: 1979, *Astron. Astrophys.* **80**, 212

Shandarin, S.F., Zeldovich, Ya.B.: 1986, in *Cosmology, Astronomy, and Fundamental Physics*, Second ESO-CERN Symposium, ed. G. Setti and L. van Hove, p. 45

Tammann, G.A.: 1978, *Mem. Soc. Astron. Ital.* **49**, 315

Tenorio-Tagle, G.: 1981, *Astron. Astrophys.* **94**, 338

Tenorio-Tagle, G., Beltrametti, M., Bodenheimer, P., Yorke, H.W.: 1982, *Astron. Astrophys.* **112**, 104

Tenorio-Tagle, G.: 1984, *Publ. Astron. Inst. Czech. Acad. Sci.* **56**, 168

Tomisaka, K., Habe, A., Ikeuchi, S.: 1981, *Astrophys. Space Sci.* **78**, 273

Viallefond, F., Allen, R.J., Goss, W.M.: 1981, *Astron. Astrophys.* **104**, 127

Viallefond, F., Goss, W.M., van der Hulst, J.M., Crane, P.C.: 1986, *Astron. Astrophys. Suppl.* **64**, 237

Weaver, R., McCray, R., Castor, J., Shapiro, P., Moore, R.: 1977, *Astrophys. J.* **218**, 377